High-resolution imaging of the dynamic tumor cell–vascular interface in transparent zebrafish

Konstantin Stoletov, Valerie Montel, Robin D. Lester, Steven L. Gonias, and Richard Klemke*

Department of Pathology and Moores Cancer Center, University of California at San Diego, 9500 Gilman Drive, MC0612, La Jolla, CA 92093

Edited by Judah Folkman, Harvard Medical School, Boston, MA, and approved September 12, 2007 (received for review April 16, 2007)

Cell metastasis is a highly dynamic process that occurs in multiple steps. Understanding this process has been limited by the inability to visualize tumor cell behavior in real time by using animal models. Here, we employ translucent zebrafish and high-resolution confocal microscopy to study how human cancer cells invade in tissues, induce angiogenesis, and interact with newly formed vessels. We use this system to study how the human metastatic gene *RhoC* promotes the initial steps of metastasis. We find that *RhoC* expression induces a primitive amoeboid-like cell invasion characterized by the formation of dynamic membrane protrusions and blebs. Surprisingly, these structures penetrate the blood vessel wall exclusively at sites of vascular remodeling and not at regions of existing intact vessels. This process requires tumor cells to secrete VEGF, which induces vascular openings, which in turn, serve as portholes allowing access of *RhoC*-expressing cells to the blood system. Our results support a model in which the early steps in intravasation and metastasis require two independent events: (*i*) dynamic regulation of the actin/myosin cytoskeleton within the tumor cell to form protrusive structures and (*ii*) vascular permeablization and vessel remodeling. The integration of zebrafish transgenic technology with human cancer biology may aid in the development of cancer models that target specific organs, tissues, or cell types within the tumors. Zebrafish could also provide a cost-effective means for the rapid development of therapeutic agents directed at blocking human cancer progression and tumor-induced angiogenesis.

angiogenesis | cancer | RhoC | metastasis

Metastasis is the major cause of death in cancer patients, and there are currently no therapeutic agents available to prevent this disease (1–2). Current models view metastasis as a highly dynamic process that occurs in multiple steps (1–3). The initial steps involve disruption of cell–cell adhesions, the migration of cells away from the primary tumor, and intravasation into the vasculature. The later steps involve tumor cells traveling to distant sites, where they must extravasate into permissible microenvironment to form secondary tumors. The individual steps in the metastatic cascade remain incompletely understood. This is especially true of the initial steps leading to intravasation, when small developing tumors and micrometastases are not easily detected. Most of our understanding of these early steps during the metastatic cascade has been derived from static images of large, advanced-stage tumors and their associated metastases. Consequently, fundamental questions remain as to how invasive cancer cells navigate through complex tissues, locate vessels, and intravasate. Thus, there is a crucial need to understand invasive mechanisms and angiogenic programs that facilitate metastasis so that therapeutic strategies can be developed to block disease progression.

Progress has also been limited by the inability of existing animal models (mouse and chick) to facilitate high-resolution imaging of the dynamic process of cell invasion and tumor cell–vascular interactions during cancer progression. These models are also labor intensive and do not provide cost-effective, efficient ways to optically screen pharmacological agents for anticancer and antiangiogenic properties. This is a particular problem, because development of an effective anticancer agent will require testing of many different compounds or combinations of compounds against a wide range of tumor types driven by different oncogenic programs. Therefore, an animal system is needed that allows fast, noninvasive, high-resolution imaging of the early stages of cancer progression and angiogenesis that can be used for therapeutic testing. Zebrafish provides an ideal vertebrate model for this application because they are optically transparent, cost-effective to maintain and breed, and are readily amenable to genetic and pharmacological screening (4). Also, comparison of the zebrafish and human genomes reveals remarkable sequence and functional conservation of cell cycle, tumor suppressor, protooncogenes, angiogenic factors, and extracellular matrix proteins (4–5).

In this study, we show that, when injected into the zebrafish peritoneal cavity, human tumor cells survive, invade within the tissue, and home to and remodel the fish vasculature. Using this model system and high-resolution confocal microscopy, we investigate how the metastatic gene *RhoC* mediates tumor cell invasion and intravasation. RhoC is a member of the Rho family of small GTPases that control the actin/myosin cytoskeleton. Amplification of this gene has been associated with cancer progression to metastatic disease and poor patient prognosis in breast, colon, and pancreatic cancer (6–9). However, the underlying mechanisms remain unclear (10). We find that RhoC expression induces a primitive amoeboid-like cell invasion characterized by the formation of dynamic membrane protrusions and blebs that penetrate vascular openings in the remodeling vascular wall. The vascular openings serve as portholes, allowing access of RhoC-expressing cells to the blood system. Our findings indicate that RhoC-induced cytoskeletal changes and the release of vascular permeability factors work cooperatively to mediate cell intravasation during the early stages of cancer cell metastasis and highlight the use of optically translucent zebrafish as a model system to visualize human cancer progression in high resolution.

Results

Analysis of Human Cancer Progression in Zebrafish. Several human cancer cell lines expressing fluorescent marker proteins (GFP, CFP, or DsRed) were injected into the peritoneal cavity of 1-month-old chemically immunosuppressed *AB* or *Tg(fli1:EGFP)* zebrafish (11). Animals were then examined for tumor formation, angiogenesis, cell invasion, and morphology as well as animal viability by using either a stereofluorescence or a confocal microscope [Fig. 1 *A–E*

Author contributions: K.S. and R.K. designed research; K.S., V.M., and R.D.L. performed research; K.S., V.M., R.D.L., S.L.G., and R.K. contributed new reagents/analytic tools; K.S., S.L.G., and R.K. analyzed data; and K.S., S.L.G., and R.K. wrote the paper.

The authors declare no conflict of interest.

This article is a PNAS Direct Submission.

Abbreviations: CAM, chicken chorioallantoic membrane; dpi, days after injection.

*To whom correspondence should be addressed. E-mail: rklemke@ucsd.edu.

This article contains supporting information online at www.pnas.org/cgi/content/full/0703446104/DC1.

© 2007 by The National Academy of Sciences of the USA

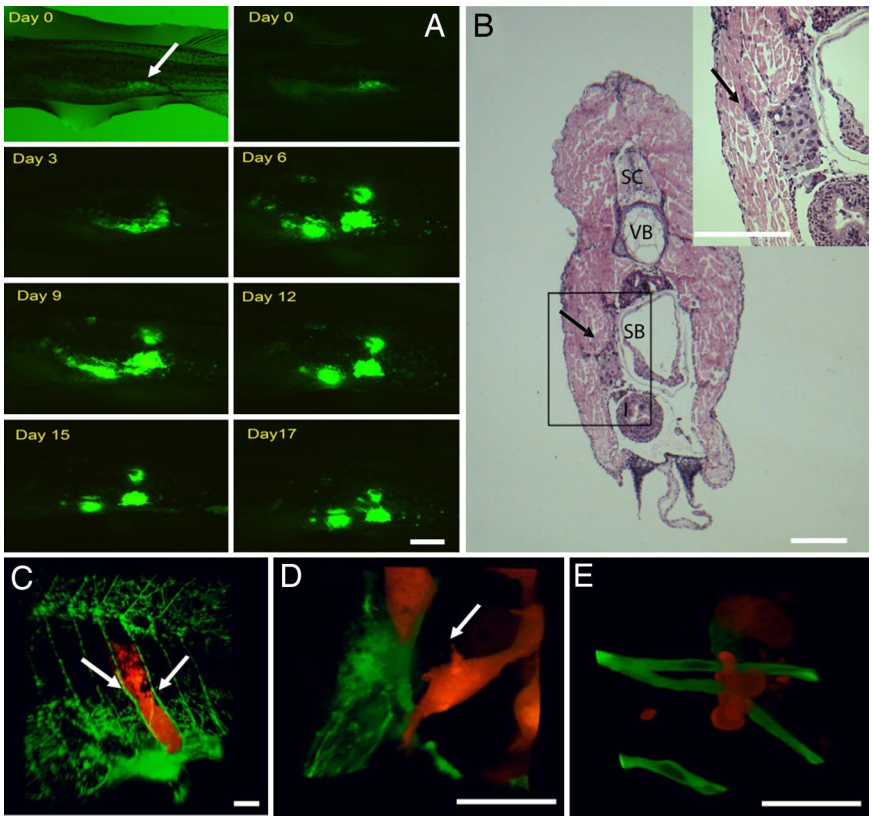

Fig. 1. Human tumor cells form microtumors in the body wall of zebrafish. (*A*) MDA-435 control cells expressing GFP were injected into the peritoneal cavity of zebrafish and imaged daily for 17 consecutive days with a fluorescence stereomicroscope. The image is representative of >100 injected animals. Arrow shows the injection site. (*B*) H&E stain of MDA-435 control cells 5 days after injection (dpi) in the body wall (cross-section). Tumor cells can be seen attached to the body wall surface (arrow). (*Inset*) High-magnification image of the box denoted in *B*. The arrow points to a group of cells invading into the body wall. SC, spinal cord; VB, vertebrae; SB, swim/air bladder. (*C*) Three-dimensional reconstruction of a microscopic MDA DsRed tumor developing in the body wall between the intersegmental vessels (arrows) of *Tg(fli1:EGFP)* fish, 4 dpi. (*D*) Three-dimensional reconstruction of single invading MDA-435 control cell. (*E*) Three-dimensional reconstruction of single invading HT1080 cell. Color code: In *A*, Human tumor cells are green; in *C–E*, fish blood vessels and green, and human tumor cells are red. [Scale bars, 1 mm (*A* and *B*); 200 μm (*C*), and 20 μm (*D* and *E*).]

and supporting information (SI) Table 1]. The optical clarity of fish tissues and the developmentally patterned vessels allowed us to mark the precise site of tumor cell inoculation and to monitor cell behavior and angiogenesis in relation to the GFP-labeled vasculature over many days in the same animal. In fact, tumorigenesis and vascular remodeling can be imaged daily (2- to 4-h intervals) for >2 weeks without adverse effects, which is a particular advantage of this model. Under these conditions, adenocarcinoma MDA-MB-435 (MDA-435), fibrosarcoma (HT1080), and melanoma (B16) cell lines form microscopic tumors that display various levels of cell invasion, angiogenesis, and animal viability, whereas nontumorigenic MEF cells do not (Fig. 1 *A–E* and SI Table 1). Also, fluorescent 10-μm beads did not move from the site of injection, induce angiogenesis, or alter animal viability (data not shown).

For most of our studies, we used the MDA-435 cell line, because they readily formed tumors (SI Table 1) in zebrafish and have been extensively characterized in the literature (12). After injection into the peritoneal cavity, MDA-435 cells readily attached to the interior side of the body wall (Fig. 1 *A* and *C*), where they displayed a steady increase in tumor size, reaching a maximum volume ($\approx$200 μm^3) on day 5–6 with a mean animal viability of 13.6 $\pm$ 0.45 days. Histological analysis and confocal microscopy of developing tumors revealed that the cells invade locally into the body wall in close association with the intersegmental vessels (Fig. 1 *B* and *C*). We did not observe extensive invasion of MDA-435 cells (>200 μm from injection site) or metastasis to distant organs. MDA-435 cells also display low metastatic behavior in a quantitative chicken chorioallantoic membrane (CAM) xenograft model when compared with other human tumor cells such as HT1080 (13). In this model, MDA-435 cells develop as compacted cell aggregates that cluster around the intersegmental vessels (Fig. 1*C*). In contrast, highly metastatic HT1080 cells (13) scattered throughout the body wall and did not form compact aggregates in association with vessels (Fig. 1*E* and SI Table 1). Also, when coinjected together with MDA-435 cells in the same animal, HT1080 cells were observed to readily invade out from the injection site into the tissue, whereas MDA-435 cells did not. In some cases, HT1080 cells were observed to invade >300 μm from injection site (SI Fig. 5). Animals injected with HT1080 cells also showed significantly reduced viability compared with MDA-435 cells, which probably results from the increased invasiveness (SI Table 1). Thus, human tumor cells form microtumors in zebrafish and display similar invasive properties in relation to other xenograft models of human cancer.

Human Tumor Cells Induce Zebrafish Angiogenesis. The developmentally patterned fish vasculature is easily visualized, making it possible to detect and quantify subtle changes in angiogenesis, before and after tumor cell inoculation (11). Approximately 20% of the developing MDA-435 tumors displayed vessel remodeling (Fig. 2 *A–C*). These vessels began to form at day 4 after injection (dpi) by looping out from preexisting vessel surfaces and contained multiple translumen walls, which is indicative of an intussusceptive type of angiogenesis (14) (Fig. 2 *A–C* and SI Movies 1 and 2). No angiogenesis was observed in control

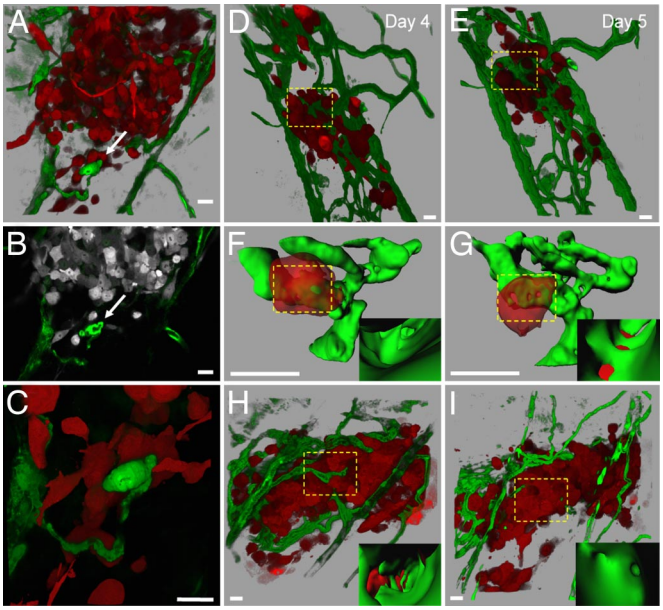

Fig. 2. Visualization of tumor-induced angiogenesis and tumor cell–vascular interactions. (*A*) Three-dimensional reconstruction of MDA-435 cell microtumor in the body wall of *Tg(fli1:egfp)* zebrafish tissue, 5 dpi. Note the remodeling vessel (white arrows in *A*–*C*). (*B*) Single optical section (1 μm) of microtumor in *A*, (SI Movie 1 shows a series of optical sections through the tumor and remodeling vessels). (*C*) High magnification of invasive cells clustering around the remodeling vessel shown in *A* and *B* (SI Movie 2). (*D* and *E*) Three-dimensional reconstruction of MDA-435 tumor cells secreting human VEGF in the body wall of *Tg(fli1:egfp)* zebrafish at 4 (*D*) and 5 (*E*) dpi. Images were obtained from the same animal on consecutive days. (*F* and *G*) Three-dimensional reconstructions of digitally isolated tumor cells in contact with host vessels from *D* and *E* (dotted squares; SI Movies 3 and 4). (*Insets*) Three-dimensional reconstructions of the vessel interior at sites of vessel openings and tumor cell membrane integration. (*H*) Three-dimensional reconstruction of a MDA-435 microtumor secreting human VEGF at 4 dpi before (*H*) and after (*I*) treatment (24 h) with 5 μm of the VEGF receptor inhibitor SU5416 (SI Movies 5 and 6). (*Insets*) Inside vessel surface within the dotted squares. Color code: Fish blood vessels are green, and human tumor cells are red (or gray in *B*). (Scale bars, 20 μm.)

animals injected with fluorescent 10-μm microspheres (data not shown) or nontumorigenic MEF cells (SI Table 1).

The low level of angiogenesis was expected because MDA-435 cells do not secrete appreciable amounts of angiogenic factors (15); therefore, we engineered MDA-435 cells to secrete human VEGF. In this case, 100% of MDA-435 tumors showed robust vessel sprouting and remodeling that led to the *de novo* appearance of vessels that completely infiltrated the tumor cell mass within 3–4 dpi (Fig. 2 *D* and *E*). Quantitative 3-D computer analysis revealed a dramatic increase in the number of branch points, total vessel length, and vessel diameter compared with MDA-435 control tumors developing in the absence of VEGF (SI Fig. 6). Importantly, the remodeling vessels displayed a tortuous, irregular shape and increased variability in vessel wall thickness (SI Fig. 7). Examination of single confocal optical sections revealed 1- to 3-μm-wide disruptions in the endothelial cell layer that appeared randomly along the surface of VEGF-induced vessels. Upon 3D reconstruction, these disruptions appeared as openings in the vessel wall surface. (Fig. 2 *F* and *G*). Interestingly, 23 ± 2.2% of VEGF-secreting tumor cells were observed to be in contact with the vascular openings. Optical sections of the tumor cell–vascular interface revealed that the tumor cells had integrated into the vascular openings of the endothelial cell layer, which is indicative of vascular mimicry (Fig. 2 *F* and *G* and SI Movies 3 and 4) (16). Despite tumor cell integration into the vessel wall, we rarely observed tumor cells protruding invadopodia into the vessel lumen, suggesting that these cells cannot efficiently intravasate. Importantly, the VEGF-induced vasculature surrounding the tumor mass was highly permeable to red fluorescent dextran (molecular mass 2 × 10^6 Da), whereas normal vessels outside the tumor area were not (SI Fig. 7). Pharmacological treatment of these animals with the VEGFR inhibitor SU5416 restored the integrity of the vessel wall. Together, these findings indicate that tumor-induced VEGF secretion can induce vascular remodeling and permeablization. Also, after the SU5416 treatment, tumor cell size decreased from 25.5 ± 1.7 to 16 ± 1.0 μm, whereas the total number of tumor cells did not change (Fig. 2 *H* and *I*, SI Fig. 7, and SI Movies 5 and 6).

RhoC Expression Induces a Highly Invasive Phenotype Characterized by Primitive Amoeboid Cell Movement. We next investigate how amplification of RhoC in MDA-435 cells alters cell invasion and angiogenesis in zebrafish. MDA-435 breast adenocarcinoma cells were engineered to stably overexpress RhoC (MDA-RhoC) and the fluorescent marker protein (DsRed). Control low-metastatic MDA-435 cells were engineered to stably express DsRed or CFP fluorescent proteins. Several prominent features distinguished MDA-RhoC cells from control MDA-435 cells. First, control cells invaded locally along the dorsoventral vessels in the body wall, where they grew as cell aggregates in close association with the existing vessels (Fig. 2 *A* and *B* and SI Movies 1 and 2). MDA-RhoC cells also invaded into the body wall but were more scattered throughout the tissue and did not closely associate with the vasculature (Fig. 3 *A* and *B* and SI Movie 7). Second, time-lapse analysis revealed that RhoC cells invade through tissues by extending small membrane projections and blebs (Fig. 3*C*). Third, computational analysis of cancer cell morphology, revealed that the majority (≈99%) of RhoC-expressing cells displayed a more round amoeboid-like shape and significantly reduced cell size, whereas control cells showed both round and elongated mesenchymal shapes with extensive invadopodia formation (Fig. 3 *D* and *E*). This response was unique to RhoC cells, because MDA-435 cells overexpressing oncogenic Src kinase did not display this invasive phenotype nor did they show extensive membrane blebbing (SI Table 1). Interestingly, we observed that the small blebs (≤2.0 μm) were ripped from the MDA-RhoC cell membrane and shed into the surrounding tissue (13.3 ± 2.3 blebs per RhoC cell compared with 3.2 ± 0.6 blebs per control cell, Fig. 3 *C* and *G*). Recent work indicates that mesenchymal cell invasion is characterized by the release of matrix proteases and matrix remodeling, whereas amoeboid invasion mechanism may be independent of extracellular matrix proteolysis (17–18). MDA-RhoC type of invasion was strikingly similar to the invasion response used by the highly metastatic HT1080 cells, which also displayed amoeboid movement and dramatic membrane blebbing (Fig. 1*E* and SI Table 1). In contrast to MDA-RhoC and HT1080 cells, control MDA-435 cells showed only local invasion by extending and retracting long membrane processes (Fig. 1*D*). Notably, there was a significant increase in the number of mesenchymal cells (68.5 ± 2.9%) residing in the outer edge of the tumor mass (≈30 μm or two cell layers) compared with those cells that reside in the inner tumor cell mass (31.5 ± 2.9%). There were also more mesenchymal cells contacting blood vessels compared with rounded cells (mesenchymal 42 ± 3.7% vs. rounded 11.6 ± 2.0%)(Fig. 2 *A*–*C*). These findings suggest the possibility that cells with a mesenchymal phenotype are involved in extracellular matrix and vessel remodeling.

MDA-RhoC Cells Do Not Change the Invasive Behavior of Neighboring Control Tumor Cells. The zebrafish model combined with confocal microscopy facilitates simultaneous imaging of two or more cell types in the same tumor. This advantage allowed us to determine whether RhoC cells altered the behavior of control cells residing within the same tumor microenvironment. It is possible that the expression of RhoC in MDA-435 cells could induce secretion of

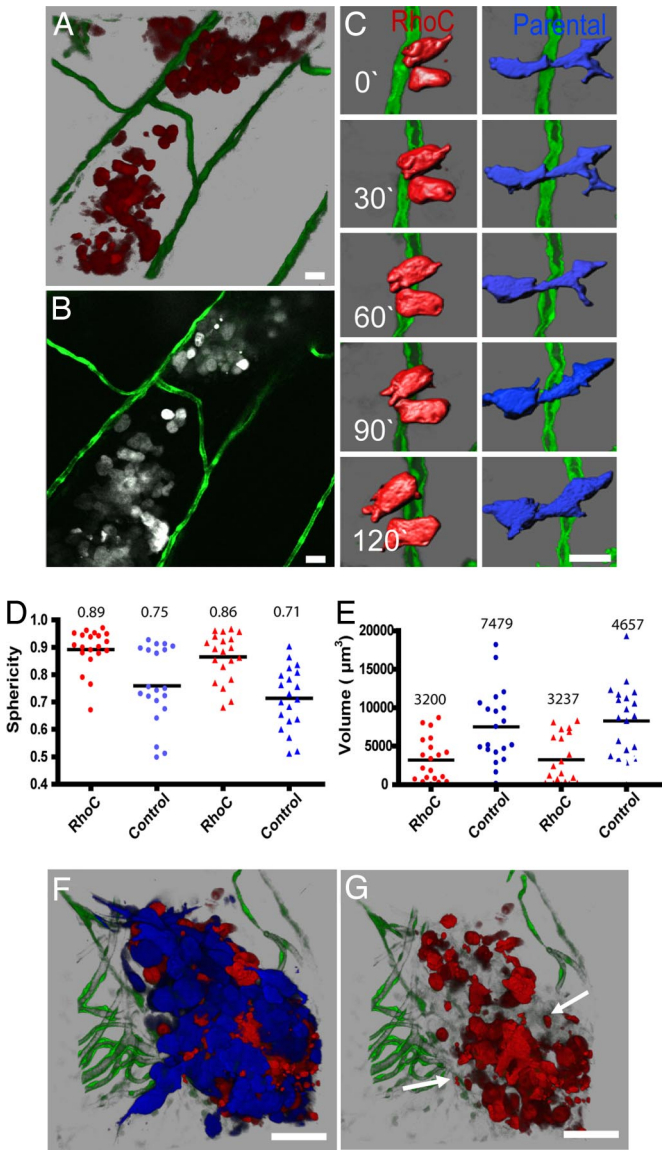

Fig. 3. RhoC-induced human tumor cell morphology and invasion. (*A*) Three-dimensional reconstruction of MDA-RhoC cells invading the body wall of *Tg(fli1:egfp)* zebrafish at 5 dpi. (*B*) Single optical section (1 μm) of cells in *A* (SI Movie 7 shows all optical sections through the tumor). (*C*) Time-lapse analysis of control MDA-435 (blue) and MDA-RhoC (red) cells invading within the body wall of *Tg(fli1:egfp)* zebrafish. Images were acquired every 15 min and reconstructed in 3-D and then digitally highlighted to reveal surface morphology by using Imaris Contoursurface. (*D* and *E*) The distribution of sphericity (round vs. elongated) (*D*) and cell volume (*E*) for MDA-435 and MDA-RhoC cells injected individually (●) or together (▲) were measured as described in *SI Text*. MDA-RhoC cells had significantly higher sphericity and lower volume ($P < 0.05$, *t* test) than MDA-control cells when injected separately or together. Horizontal lines represent mean values displayed above the plots. (*F*) Three-dimensional reconstruction of MDA-435 (blue) and MDA-RhoC cells (red) coinjected at a 1:1 ratio at 3 dpi. (*G*) Three-dimensional reconstruction of *F*, but only MDA-RhoC cells (red channel) are shown. Arrows indicate membrane blebs shed into the surrounding tissue. Color code: Fish blood vessels are green; in *B–G*, MDA-RhoC cells are red (or gray in *B*), and MDA parental cells are blue. (Scale bars, 20 μm.)

various cytokines and proteases capable of altering the invasive properties of neighboring control tumor cells (19). To investigate this possibility, DsRed-MDA-RhoC cells and MDA-CFP controls cells were coinjected into *Tg(fli1:egfp)* zebrafish at a 1:1 ratio to create a mosaic tumor (Fig. 3 *F* and *G*). MDA-RhoC cells did not

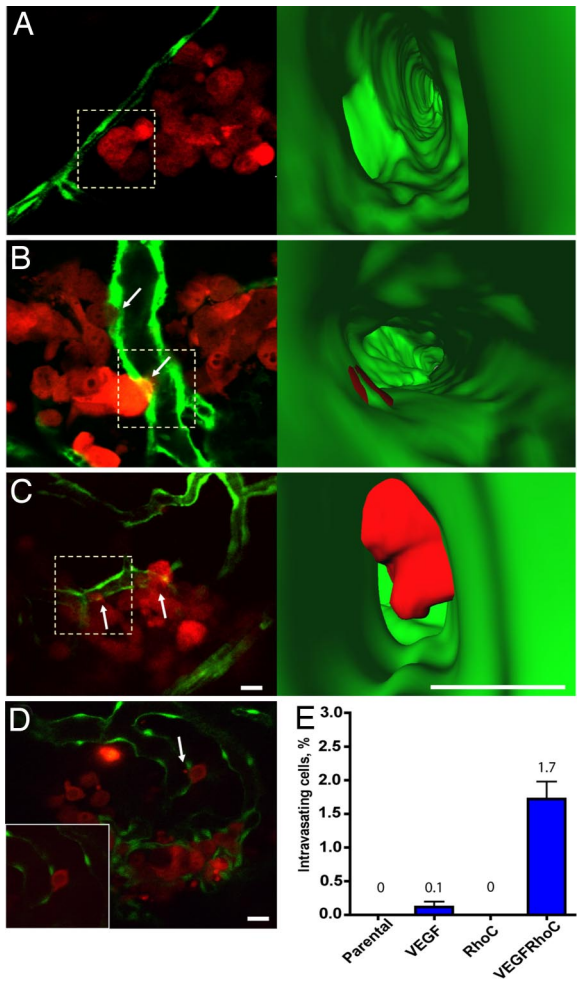

Fig. 4. RhoC cooperates with VEGF to enhance tumor cell intravasation. Single optical sections showing tumor cells interacting with the vessel surface (5 dpi). (*A–C*) MDA-435 expressing RhoC (*A*), VEGF (*B*), or RhoC and VEGF (*C*). (*Right*) Three-dimensional reconstructions of interior vessel surfaces at the tumor cell-vessel interface (dotted squares in *Left*). Arrows show vascular mimicry (*B*) or membrane protrusion into the vessel lumen (*C*). In *C*, note the large increase in the membrane protrusion inside the vessel lumen of the MDA-RhoC cells secreting VEGF (SI Movies 8–10). (*D*) Single optical section showing an MDA-RhoC VEGF membrane protrusion in the vessel lumen (arrow). (*Inset*) The same cell 5 min later. (*E*) Plot showing percent of intravasating cells for parental MDA-435 cells or MDA-435 cells expressing VEGF, RhoC, or RhoC and VEGF. MDA-RhoC cells that express VEGF had a significantly higher percentage of intravasating cells ($P < 0.05$, *t* test) than other cell types. Mean and SEM values are displayed above the plot. Colors code: Fish vasculature is green, and human tumor cells are red. [Scale bars, 20 (*Left*) or 10 μm (*Right*).]

alter the morphology, mode of invasion, or migration speed ≈10 μm/hr) of control cells, nor did the control cells alter the invasive behavior of RhoC cells (Fig. 3 *F* and *G*). Thus, the invasive mechanisms mediated by RhoC cells are intrinsic and do not influence other tumor cells through matrix remodeling or the release of paracrine factors into the local microenvironment. Together these findings demonstrate that the MDA-RhoC cells use amoeboid migration to invade tissues independent of the vascular network, whereas invading control cells use mesenchymal migration to invade locally in close association with blood vessels.

RhoC and VEGF Work Cooperatively to Mediate Cancer Cell Intravasation. The finding that RhoC-induced cell invasion occurred independently of tumor cell-vessel interactions was surprising because highly invasive tumors often display increased vascular

remodeling and angiogenesis. We reasoned that RhoC amplification may contribute to metastasis at later stages after the angiogenic switch has been triggered by VEGF secretion (20). To investigate this possibility, we engineered MDA-RhoC and control cells to secrete human VEGF and injected these cells into *Tg(fli1:egfp)* zebrafish. Surprisingly, VEGF secretion altered the pattern of the MDA-RhoC-mediated radial invasion to directed invasion in close association with remodeling vessels (Fig. 4*A*). Most importantly although, we found that when MDA-435 cells express VEGF and RhoC together they were able to protrude large membrane extensions (5 μm or greater) into the vessel lumen. The number of cells that displayed this phenotype was significantly higher ($P < 0.05$) compared with cells expressing RhoC or VEGF alone (Fig. 4 *A–E* and SI Movies 8–10). In a few of these cells, we were able to observe the cellular protrusions being ripped from the cell surface because of blood flow (Fig. 4*D*). The ability of MDA-RhoC cells to protrude membrane extensions into VEGF-induced vascular openings suggests that these cells have acquired the unique ability to intravasate. Because the small vessels in the zebrafish body wall and the low numbers of injected cells may not be amenable to full cell intravasation, we measured RhoC-mediated intravasation using a modified chick CAM model that facilitates growth of MDA-435 adenocarcinoma cells and confocal imaging of intravasation (*Experimental Procedures*, 13). In this case, mosaic tumors of MDA control and RhoC cells were allowed to grow on the chick CAM for 10 days. Optical sectioning and 3-D rendering of the tumor cell vascular interface revealed that RhoC cells had an 8 fold increase in intravasation compared with control MDA-435 cells ($P < 0.05$; SI Fig. 8). MDA-RhoC tumor cell intravasation in chick CAM was also dependent on the VEGFR signaling because it was inhibited by the treatment of chick CAMs with SU5416 (SI Fig. 8). Together, our findings indicate that RhoC amplification contributes to tumor cell intravasation by increasing membrane protrusions capable of penetrating VEGF-induced vascular openings in the vessel wall. Thus, RhoC and VEGF work cooperatively to facilitate invasion and intravasation through regulation of the dynamic actin–myosin cytoskeleton and vascular remodeling, respectively.

Discussion

The zebrafish xenograft model described here provides a unique window to view the early steps in tumor formation, angiogenesis, cell invasion, and intravasation with unprecedented clarity. Significant evidence is accumulating that demonstrates remarkable functional conservation of human and zebrafish vascular biology (4, 11). Indeed, most of the proangiogenic genes have been described in fish including *VEGF A* and *C*, *bFGF*, *ang1*-2, *tie1*-2, *ephrin* B2, and *Notch*. Our observation that tumor cells secreting human VEGF strongly promote fish vessel remodeling and angiogenesis supports these findings and points to zebrafish as a suitable model to investigate conserved mechanisms of human tumor-induced angiogenesis (21–25).

Recently, zebrafish has emerged as a useful model for therapeutic drug research and preclinical studies (4). Several unique features make this animal an attractive model to test cancer therapeutics. Zebrafish are inexpensive to maintain, breed in large numbers, develop rapidly *ex vivo*, and can be maintained in small volumes of water (26–27). In our studies, we found that treatment of *Tg(fli1:egfp)* transgenic animals with physiologically relevant doses of the VEGF receptor kinase inhibitor SU5412 potently blocked the host's angiogenic response to tumor-secreted human VEGF. An intriguing observation in our study was the formation of vascular holes induced by tumor-derived VEGF. These structures appeared randomly along the remodeling vessel wall independent of direct tumor cell–vascular interactions and required VEGFR signaling. Although it is not yet clear how these structures form, it may involve Src kinase signaling, which has been shown to operate downstream of the VEGFR to mediate vascular permeability (28–30). Interestingly, in the mouse, extravasating tumor cells were observed by transmission EM to protrude membrane processes through small 1- to 2-μm openings between adjacent endothelial cells. This response was also significantly enhanced when the tumor cells were induced to secrete VEGF (30).

Another effect of VEGF-mediated vascular disruption may be the release of blood-borne chemotactic factors into the tumor microenvironment. These factors could provide guidance cues to direct invasive cells to areas of remodeling vessels (30). The fact that the secretion of VEGF by RhoC cells redirected their invasion from scattered movement to more localized invasion in close association with remodeling vessels supports this notion. Also, the ability of RhoC to increase cell scattering within tissues would be expected to increase the invasive range of cells. This would increase its chance of locating regions of vascular remodeling providing a metastatic advantage.

Our data demonstrate that, once an invasive cell arrives at a site of vessel remodeling, it can physically dock onto vascular openings. Optical sectioning and 3-D rendering revealed that these cells either intercalate their membranes into the vascular wall, as was the case with the low-metastatic control cells, or protrude large membrane processes that completely penetrate into the vessel lumen, as was the case with the metastatic RhoC cells. These findings suggest that RhoC amplification in tumor cells provides a metastatic advantage by forming unique invasive structures capable of penetrating vessel openings. This process likely involves regulation of the dynamic actin-myosin cytoskeleton through RhoC's ability to regulate the ROCK and MLC-phosphatase pathway as demonstrated (10). Interestingly, RhoC's close homologue RhoA was recently shown to promote amoeboid movement of MDA-435s cells, suggesting that RhoA and RhoC may contribute to this response (6, 31). Collectively, these studies suggest that the release of VEGF by invasive tumor cells disrupts endothelial cell–cell connections which create vascular disruptions which serve as portholes for cell intravasation. This, combined with activation of metastatic programs like RhoC that regulate protrusive structures, could provide the proper conditions for cell intravasation. However, RhoC probably is not involved in the early stages of cell transformation and tumor formation (32) and may not provide a strong angiogenic switch *in vivo* (SI Table 1). These findings point to RhoC's being a late activating metastatic gene that operates after the angiogenic switch has been already triggered. Recently, another prometastatic gene *twist* was shown to be specifically involved in the intravasation step of metastasis. Interestingly *twist* has also been shown to promote VEGF secretion by human breast cancer cells, suggesting that twist and RhoC may work through similar mechanisms (33, 34).

The use of zebrafish as xenograft model of human cancer affords high-resolution imaging capabilities and incorporates the power of zebrafish genetics with the large knowledge base and tool chest of human cancer biology. The recent development of transgenic zebrafish models of cancer progression and the ability to propagate human cancer cells in zebrafish (35–39) will provide a valuable vertebrate system to unravel the mechanisms of human cancer and to develop cancer therapeutics.

Experimental Procedures

Cell Lines and Constructs. Stable fluorescent tumor cell lines were generated by transfection with pGFP-N1, pDsRed-N1, or pCFP-N1 vectors (Invitrogen, Carlsbad, CA) by using Lipofectamine reagent (Invitrogen), followed by FACS sorting. Human RhoC was cloned into pLentiCMVMCS (puromycin). RhoC encoding viral particles were used for infection of MDA-435 (DsRed) cells, whereas MDA-435 cells were infected with empty vector virus. RhoC was overexpressed 5- to 10-fold above the endogenous level as measured by Western blotting as described (40). Recombinant human VEGF adenoviral vector (Cell Biolabs, San Diego, CA) was used at a 100 multiplicity of infection for MDA-435 infection.

Animal Preparation and Injection of Human Tumor Cells. Animals were maintained according to the University of California at San Diego animal welfare guidelines as described (41). Zebrafish (25–35 days old) were immunosuppressed with 10 μg/ml dexamethasone for 2 days (36) and anesthetized by 0.003% Tricaine. Fifty to 300 cells or 10-μm beads (Molecular Probes, Eugene, OR) suspended in PBS were injected into the peritoneal cavity by using an Eppendorf Cell Tram Vario injector equipped with a 0.75-mm borosilicate glass needle (L = 50 mm, diameter of the needle opening = 20 μm). The injected fish was washed once with water and transferred to 6-well dishes containing 5 ml of water with 10 μg/ml dexamethasone. Water was changed daily, and fish were fed twice a day with brine shrimp and maintained by using normal fish husbandry conditions (41).

Pharmacological Treatment of Fish with SU5416. SU5416 (Calbiochem, San Diego, CA) was added directly to the water at a final 5 μM concentration. DMSO was used as a vehicle control. Animals were maintained in 2–5 ml of water that was changed daily.

Fluorescent Dextran Injection. Zebrafish were anesthetized by 0.003% Tricaine 4 days after tumor cell injection. We modified a protocol used for dextran injection into the mouse vasculature (42). Dextran-Texas red (0.5 μl) in PBS (5 mg/ml, molecular mass, 2×10^6 Da; Molecular Probes) was injected into the caudal vein by using an Eppendorf Cell Tram Vario injector equipped with a 0.75-mm borosilicate glass needle (L = 50 mm, diameter of the needle opening = 5 μm). Injected fish were washed once with water and transferred to Petri dish with water for 1 hour. Fish were imaged 1 hour later.

Microscopy and Tumor Cell Imaging. Anesthetized fish were imaged in a small drop of Tricaine (0.003%) containing water on a glass coverslide. For *in vivo* confocal microscopy, anesthetized fish were housed in a sealed, temperature-controlled chamber (20/20 Technologies, Laval, QC, Canada) in a small drop of Tricaine-containing water. We used MRC 2100 (Bio-Rad, Hercules, CA) or C1-si confocal (Nikon, East Rutherford, NJ) microscopes. Excitation was 488 nm for GFP, 561 nm for DsRed, and 408 nm for CFP. For each 3D image, 0.5–2 μm step z-stacks (512×512 focal planes, 20–100 μm in depth) were acquired over a 1- to 3-min period by using 10× (Nikon , N.A. 0.45), 40× (S Fluor, N.A. 0.9), or 60× (Plan Apo, WI, N.A. 1.2) objectives. For time series experiments, animals were kept under the anesthesia for up to 4 h.

Intravasation of Breast Cancer Cells in CAMs. A detailed protocol can be found in *SI Text*.

Histology. Tumor-injected zebrafish was fixed in formalin and embedded in paraffin and stained with H&E by using standard methods.

Statistical Analysis. All of the data were analyzed by using GraphPad Prizm software (www.graphpad.com) for statistical significance. Data plots show mean values (above the plots) ± SEM except Fig. 3 *D* and *E* and SI Fig. 7*E* that show distributions of single measurements and mean values (horizontal lines and above the plots). For animal numbers used in experiments and more details on the quantification methods used, see *Data Analysis and Quantification* in *SI Text*.

We are grateful to Dr. Oliver Pertz (University of California at San Diego) for making RhoC constructs, Monica Holcomb (Biogen IDEC, Cambridge, MA) for help with the zebrafish culture, Dr. Bill Kiosses (The Scripps Research Institute, La Jolla, CA) for help with confocal microscopy, the J. Belmonte laboratory (Salk Institute, La Jolla, CA) for help with zebrafish culture, and Patricia McGrath (Phylonix, Cambridge, MA) for discussion of the manuscript. This work was supported by California Breast Cancer Research Program Postdoctoral Fellowship 11FB-0088 (to K.S.) and National Institutes of Health Grants GM068487 and CA097022 (to R.K.) and CA94900 to (to S.L.G.).

1. Gupta PB, Mani S, Yang J, Hartwell K, Weinberg RA (2005) *Cold Spring Harb Symp Quant Biol* 70:291–297.
2. Gupta G, Massaque J (2006) *Cell* 127:679–695.
3. Condeelis J, Segall JE (2003) *Nat Rev Cancer* 3:921–930.
4. Zon LI, Peterson RT (2005) *Nat Rev Drug Discov* 4:35–44.
5. Berghmans S, Jette C, Langenau D, Hsu K, Stewart R, Look T, Kanki JP (2005) *BioTechniques* 39:227–237.
6. Clark EA, Golub TR, Lander ES, Hynes RO (2000) *Nature* 406:532–535.
7. van Golen KL, Wu ZF, Qiao QT, Bao LW, Merajver SD (2000) *Cancer Res* 60:5832–5838.
8. Bellovin DI, Simpson KJ, Danilov T, Maynard E, Rimm DL, Oettgen P, Mercurio AM (2006) *Oncogene* 25:6959–6967.
9. Suwa H, Ohshio G, Imamura T, Watanabe G, Arils S, Imamura M, Narumiya S, Hia, H, Fukomoto M (1998) *Br J Cancer* 77:147–152.
10. Ridley AJ (2006) *Trends Cell Biol* 16:522–529.
11. Isogai S, Lawson ND, Torrealday S, Horiguchi M, Weinstein BM (2003) *Development (Cambridge, UK)* 130:5281–5290.
12. Price JE, Zhang RD (1990) *Cancer Metastasis Rev* 8:285–297.
13. Zijlstra A, Mello R, Panzaarella G, Aimes RT, Hooper JD, Marchenko ND, Quigley JP (2002) *Cancer Res* 62:7083–7092.
14. Patan S, Tanda S, Roberge S, Jones RC, Jain RK, Munn LL (2001) *Circ Res* 89:732–739.
15. Blancher C, Moore JW, Talks KL, Houlbrook S, Harris AL (2000) *Cancer Res* 60:7106–7113.
16. di Tomaso E, Capen D, Haskell A, Hart J, Loggie JJ, Jain RK, McDonald DM, Jones R, Munn LL (2005) *Cancer Res* 65:5740–5749.
17. Wolf K, Mazo I, Leung H, Engelke K, von Adrian UH, Deryugina EI, Strongin AY, Bröcker EB, Friedl P (2003) *J Cell Biol* 160:267–277.
18. Friedl P, Bröcker EB (2000) *Cell Mol Life Sci* 20:41–64.
19. van Golen KL, Wu ZF, Qiao XT, Bao L, Merajver SD (2000) *Neoplasia* 2:418–425.
20. Naumov GN, Akslen LA, Folkman J (2006) *Cell Cycle* 5:1779–1787.
21. Covassin LD, Villefranc JA, Kacergis MC, Weinstein BM, Lawson ND (2006) *Proc Natl Acad Sci USA* 103:6554–6559.
22. Küchler AM, Gjini E, Peterson-Maduro J, Cancilla B, Wolburg H, Schulte-Merker S (2006) *Curr Biol* 16:1244–1248.
23. Abe G, Ide H, Tamura K (2007) *Dev Biol* 304:355–366.
24. Lyons MS, Bell B, Stainier D, Peters KG (1998) *Dev Dyn* 212:133–140.
25. Leslie JD, Ariza-McNaughton L, Bermange AL, McAdow R, Johnson SL, Lewis J (2007) *Development (Cambridge, UK)* 134:839–844.
26. Parng C (2005) *Curr Opin Drug Discov Devel* 8:100–106.
27. Parng C, Seng WL, Semino C, McGrath P (2002) *Assay Drug Dev Technol* 1:41–48.
28. Gavard J, Gutkind JS (2006) *Nat Cell Biol* 8:1223–1234.
29. Jain RK (2002) *Semin Oncol* 29:3–9.
30. Weis S, Cui J, Barnes L, Cheresh D (2004) *J Cell Biol* 167:223–229.
31. Demou ZN, Awad M, McKee T, Perentes JY, Wang X, Munn LL, Jain RK, Boucher Y (2005) *Cancer Res* 65:5674–5682.
32. Hakem A, Sanchez-Sweatman O, You-Ten A, Duncan G, Wakeham A, Khokha R, Mak TW (2005) *Genes Dev* 19:1974–1979.
33. Yang J, Mani SA, Donaher JL, Ramaswamy S, Itzykson RA, Come C, Savagner P, Gitelman I, Richardson A, Weinberg RA (2004) *Cell* 117:927–939.
34. Mironchik Y, Winnard PT, Jr, Vesuna F, Kato Y, Wildes F, Pathak AP, Kominsky S, Artemov D, Bhujwalla Z, Van Diest P, *et al.* (2005) *Cancer Res* 65:10801–10809.
35. Sabaawy HE, Azuma M, Embree LJ, Tsai HJ, Starost MF, Hickstein DD (2006) *Proc Natl Acad Sci USA* 103:15166–15171.
36. Langenau DM, Feng H, Berghmans S, Kanki JP, Kutok JL, Look AT (2005) *Proc Natl Acad Sci USA* 102:6068–6074.
37. Haldi M, Ton C, Seng WL, McGrath P (2006) *Angiogenesis* 9:139–151.
38. Nicoli S, Ribatti D, Cotelli F, Presta M (2007) *Cancer Res* 67:2927–2931.
39. Lee LM, Seftor EA, Bonde G, Cornell RA, Hendrix MJ (2005) *Dev Dyn* 233:1560–1570.
40. Simpson KJ, Dugan AS, Mercurio AM (2004) *Cancer Res* 64:8694–8701.
41. Nusslein-Volhard C, Dahm R (2002) *Zebrafish: A Practical Approach* (Oxford Univ Press, Oxford, UK), Ed 1.
42. Nagy JA, Feng D, Vasile E, Wong WH, Shih SC, Dvorak AM, Dvorak HF (2006) *Lab Invest* 86:767–780.